

## PARTICLE ACCELERATION BY COLLISIONLESS SHOCKS CONTAINING LARGE-SCALE MAGNETIC-FIELD VARIATIONS

F. GUO , J. R. JOKIPII AND J. KÓTA

Department of Planetary Sciences and Lunar and Planetary Laboratory, University of Arizona,  
1629 E. University Blvd. Tucson AZ 85721

*Draft version November 6, 2018*

### ABSTRACT

Diffusive shock acceleration at collisionless shocks is thought to be the source of many of the energetic particles observed in space. Large-scale spatial variations of the magnetic field has been shown to be important in understanding observations. The effects are complex, so here we consider a simple, illustrative model. Here, we solve numerically the Parker transport equation for a shock in the presence of large-scale sinusoidal magnetic-field variations. We demonstrate that the familiar planar-shock results can be significantly altered as a consequence of large-scale, meandering magnetic lines of force. Because perpendicular diffusion coefficient  $\kappa_{\perp}$  is generally much smaller than parallel diffusion coefficient  $\kappa_{\parallel}$ , the energetic charged particles are trapped and preferentially accelerated along the shock front in the regions where the connection points of magnetic field lines intersecting the shock surface converge, and thus create the “hot spots” of the accelerated particles. For the regions where the connection points separate from each other, the acceleration to high energies will be suppressed. Further, the particles diffuse away from the “hot spot” regions and modify the spectra of downstream particle distribution. These features are qualitatively similar to the recent Voyager’s observation in the Heliosheath. These results are potentially important for particle acceleration at shocks propagating in turbulent magnetized plasmas as well as those which contain large-scale nonplanar structures. Examples include anomalous cosmic rays accelerated by the solar wind termination shock, energetic particles observed in propagating heliospheric shocks, and galactic cosmic rays accelerated by supernova blast waves, etc.

*Subject headings:* acceleration of particles - cosmic rays - shock waves - magnetic field

### 1. INTRODUCTION

Collisionless shocks in space and other astrophysical environments are efficient accelerators of energetic charged-particles. Diffusive shock acceleration (hereinafter DSA; Krymsky 1977; Axford et al. 1977; Bell 1978; Blandford & Ostriker 1978), is the most popular theory for charged-particle acceleration. It naturally predicts a universal power-law distribution  $f \propto p^{-\gamma}$  with  $\gamma \sim 4.0$  for strong shocks, where  $f$  is the phase-space distribution function, close to what observed in cosmic rays in many different regions of space. The basic conclusions of DSA can be drawn from the Parker transport equation (Parker 1965) by considering the shock to be a compressive discontinuity in an infinite one-dimensional and time steady system. DSA is thought to be the mechanism that accelerates anomalous cosmic rays (ACRs) in the Heliospheric termination shock and also galactic cosmic rays (GCRs) with energy up to at least  $10^{15}$  eV in supernova blast waves. However, recent *in situ* observations in the termination shock and the Heliosheath by *Voyager* 1 (Stone et al. 2005) found the intensity of ACRs is not peaked at the termination shock and the energy spectrum is still unfolding after entering the Heliosheath, which strongly indicates the simple planar shock model is inadequate to interpret the acceleration of ACRs. Numerical and analytical studies suggest the possible solution can be made by considering the temporary and/or spatial variation (Florinski & Zank 2006; McComas & Schwadron 2006; Jokipii & Kóta 2008; Kóta & Jokipii 2008; Schwadron et al. 2008). In particular, McComas & Schwadron (2006) discussed the im-

portance of the magnetic geometry of a blunt shock on particle acceleration. They argued that the missing ACRs at the nose of the Heliospheric termination shock is due to particle energization occurring primarily back along the flanks of the shock where magnetic field lines have had a longer connection time and higher injection efficiency. Kóta & Jokipii (2008) presented a more sophisticated simulation which gives results similar to that described by McComas & Schwadron (2006). Schwadron et al. (2008) also developed a 3-D analytic model for particle acceleration in a blunt shock, including perpendicular diffusion and drift motion due to large-scale shock structure.

Large-scale magnetic field line meandering is ubiquitous in the heliosphere and other astrophysical environments (Jokipii 1966; Jokipii & Parker 1969; Parker 1979). The acceleration of charged-particles in collisionless shocks has been shown to be strongly affected by magnetic-field turbulence at different scales (Giacone 2005a,b; Giacalone & Neugebauer 2008; Guo & Giacalone 2010). The large-scale magnetic field variation will have important effects on the shock acceleration since the transport of charged particles is different in the direction parallel and perpendicular to the magnetic field, as shown in early work (Jokipii 1982, 1987). The blunt shocks and shocks with fluctuating front (Li & Zank 2006) which have the similar geometry, are also relevant to this problem. In this study we consider the effect of the large-scale spatial variation of magnetic field on DSA.

## 2. BASIC CONSIDERATIONS AND NUMERICAL MODEL

The diffusive shock acceleration (DSA) can be studied by solving the Parker transport equation (Parker 1965), which describes the evolution of the quasi-isotropic distribution function  $f(x_i, p, t)$  of energetic particles with momentum  $p$  dependent on the position  $x_i$  and time  $t$  including effects of diffusion, convection, drift, acceleration and source particles:

$$\frac{\partial f}{\partial t} = \frac{\partial}{\partial x_i} \left[ \kappa_{ij} \frac{\partial f}{\partial x_j} \right] - U_i \frac{\partial f}{\partial x_i} - V_{d,i} \frac{\partial f}{\partial x_i} + \frac{1}{3} \frac{\partial U_i}{\partial x_i} \left[ \frac{\partial f}{\partial \ln p} \right] + Q \quad (1)$$

Here  $\kappa_{ij}$  is the diffusion coefficient tensor,  $U_i$  is the convection velocity and  $Q$  is a local source. The drift velocity is given by  $\mathbf{V}_d = (pcw/3q)\nabla \times (\mathbf{B}/B^2)$ , where  $w$  is the velocity of the particle,  $c$  is the speed of light, and  $q$  is the electric charge of the particle.

Kóta & Jokipii (2008) and Kóta (2010, manuscript to be submitted) considered analytically a model in which the upstream magnetic field was a plane (say,  $x, y$ ), with average direction in the  $y$  direction. The  $x$ -component of the magnetic field was composed of uniform sections (straight field lines) alternating in sign, which were periodic in  $y$ . They find “hot spots” and spectral effects which illustrate the effect of an upstream meandering in the magnetic field.

Here, we consider a 2-D ( $x, z$ ) system with a planar shock at  $x = 0$ , and a sinusoid magnetic field  $\mathbf{B} = \mathbf{B}_0 + \sin(kz)\delta\mathbf{B}$ . For most of the parts in this paper we discuss the case shown in Figure 1. In this figure, the magnetic lines of force are illustrated by blue lines. The shock is denoted by the red dashed line. The system is periodic in the  $z$  direction, with the magnetic field convecting from upstream ( $x < 0$ ) to downstream ( $x > 0$ ). In the shock frame, the particles will be subjected to convection and diffusion due to the flow velocities  $U_1$  (upstream) and  $U_2$  (downstream) and diffusion coefficients parallel and perpendicular to large scale magnetic field ( $\kappa_{1(\parallel, \perp)}$  and  $\kappa_{2(\parallel, \perp)}$ ), respectively. The gradient and curvature drifts in this case are only in the direction out of the  $x - z$  plane and thus irrelevant to this study. Because of the steady velocity difference between upstream and downstream, charged particles which travel through the shock layer will be accelerated. However, since we consider the large-scale magnetic field variation, transport of energetic particles in the fluctuating magnetic field become important. The diffusion coefficient in the  $x - z$  system can be expressed as:

$$\kappa_{ij} = \kappa_{\perp} \delta_{ij} - \frac{(\kappa_{\perp} - \kappa_{\parallel}) B_i B_j}{B^2} \quad (2)$$

The normalization units chosen in this study are: the spatial scale  $X_0 = 10$  AU, the upstream velocity  $U_1 = 500$  km/s, the time scale  $T_0 = 3 \times 10^6$  sec and the diffusion coefficients are in unit of  $\kappa_0 = 7.5 \times 10^{21} \text{cm}^2/\text{s}$ . The shock compression ratio  $r = U_1/U_2$  is taken to be 4.0. The shock layer is considered to be a sharp variation  $U_x = (U_1 + U_2)/2 - (U_1 - U_2)\tanh(x/th)/2$  with thickness  $th = 1 \times 10^{-3}$ , which is required to be less than  $\kappa_{xx1}/U_1$  everywhere in the upstream simulation domain, where  $\kappa_{xx1}$  is the upstream diffusion coefficient normal

to the shock surface. The simulation domain is taken to be  $[-2.0 < x < 2.0, -\pi < z < \pi]$ . The parallel diffusion coefficients upstream and downstream are assumed to be the same and taken to be  $\kappa_{\parallel 1} = \kappa_{\parallel 2} = 0.1$  at  $p = p_0$ . The ratio between parallel diffusion coefficient and perpendicular diffusion coefficient is taken to be  $\kappa_{\perp}/\kappa_{\parallel} = 0.05$ , which is consistent with that determined by integrating the trajectories of test particles in magnetic turbulence models (Giacalone & Jokipii 1999). The momentum dependence of the diffusion coefficient is taken to be  $\kappa \propto p^{4/3}$ , corresponding to non-relativistic particles in a Kolmogorov turbulence spectrum (Jokipii 1971). The time step is  $1 \times 10^{-7}$ , which is small enough to resolve the variation of  $U_x$  at the finite shock layer. We use a stochastic integration method, which is described in the Appendix, to obtain the numerical solution of the transport equation. The pseudo-particles are injected at the shock with initial momentum  $p_0$ , and will be accelerated if they cross the shock. Particles which move past the upstream or downstream boundaries will be removed from the simulation. The system is periodic in the  $z$ -direction, so a pseudo-particle crossing the boundaries in  $z$  will re-appear at the opposite boundary and continue to be followed. A particle splitting technique similar to (Giacalone 2005a) is used in order to improve the statistics. Although we use very approximate parameters, we note that the results are insensitive to the precise numbers.

## 3. RESULTS AND DISCUSSION

### 3.1. A shock propagating perpendicular to the average magnetic field

Consider first the case where the average magnetic field is in the  $z$ -direction and the fluctuating magnetic field is  $\delta B = B_0$ . As shown in Figure 1, the magnetic field is convected through the shock front and is compressed in the  $x$  direction, thus  $B_{z2} = rB_{z1}$ . For the sinusoid magnetic field considered in this paper, the local angle between upstream magnetic field and shock normal,  $\theta_{Bn}$ , will vary along the shock surface. As a magnetic field line passes through the shock surface, its connection points (the points where the field lines intersect the surface of the shock) will be moving apart in the middle of the plane ( $z = 0$ ) and approaching each other on the both sides of the system ( $|z| = \pi$ ). Since,  $\kappa_{\parallel} \gg \kappa_{\perp}$ , the particles tend to remain on the magnetic field lines. Because the acceleration only occurs at the shock front, as the magnetic lines of force convect downstream, the particles will be trapped and accelerated at places where the connection points converge toward each other, leading to further acceleration. For the regions where the field lines separate from each other, the particles are swept away from those regions. Figure 2 displays the spatial distribution contours of accelerated particles in three energy ranges:  $3.0 < p/p_0 < 4.0$  (top),  $8.0 < p/p_0 < 10.0$  (middle), and  $15.0 < p/p_0 < 30.0$  (bottom). The density is represented by the number of particles in simulation and its unit is arbitrary. It can be seen that “hot spots” form in the regions that connection points approaching each other at all energy ranges, with lobes extend along the magnetic field lines. The density of the accelerated particles at the connection-point separating region (in the middle of the plane) is clearly much smaller, although

there is still a concentration of low-energy accelerated particles there since the acceleration of low-energy particles is rapid and efficient at perpendicular shocks. At higher energy ranges (middle and bottom), the lack of accelerated particles may be interpreted as due to the fact that the acceleration to high energies takes time.

Figure 3 illustrates the profiles of the density of accelerated particles for different energy ranges at  $z = 0$  (top) and  $z = \pi$  (bottom). In each panel, the black solid lines show the density of low energy particles ( $3.0 < p/p_0 < 4.0$ ), the blue dashed lines show the density of intermediate energy particles ( $8.0 < p/p_0 < 10.0$ ), and red dot dashed lines show the density of particles with high energies ( $15.0 < p/p_0 < 30.0$ ). In connection-point separating regions  $z = 0$  (top), it can be seen that while the downstream distribution of low energy particles is roughly a constant, the density of particles with higher energies increase as a function of distance downstream from the shock. These particles are not accelerated at the shock layer in the center of the plane but in the “hot spots”. At  $z = \pi$  (bottom), the density of particles of all energies decreases as a function of distance, which indicates the accelerated particles diffusive away from the “hot spots”. Since the high energy particles have larger diffusion coefficients than the particles with low energy, it is easier for them to transport to the middle of the plane. The profile at  $z = 0$  is similar to *Voyager*’s observation of anomalous cosmic rays (ACRs) at the termination shock and the Heliosheath (Stone et al. 2005; Cummings et al. 2008) which shows the intensity of the ACRs is still increasing and the energy spectrum is unfolding over a large distance after entering the Heliosheath. The same physics has discussed by Jokipii & Kóta (2008), where “hot spot” of energetic particles is produced by the spatial variation of the injection of the source particles. In our current work, the concentration of energetic particles are a consequence of particle accelerated in a shock containing large-scale magnetic variation.

The top panel in Figure 4 represents the positions in  $z$  direction and the times as soon as the particles reached a certain momentum  $p_c = 3p_0$ . We show that particles are accelerated mainly at the connection-point converging region. There are also particles accelerated at middle of the plane because the particles can gain energy rapidly at perpendicular or highly oblique shock due to the smallness of perpendicular diffusion coefficient (Jokipii 1987), however, the further acceleration is suppressed by the effect that the charged particles travel away from the connection-point separating region, see also the top panel in Figure 5. It is clear that since the particles tend to follow the magnetic field lines, when the field line connection points separate from each other as field convects through the shock, the particles travel mainly along magnetic field and away from the middle of the plane. The characteristic time for a field line convect from upstream to downstream  $\tau_c = D/U_1 \sim 1$ , therefore there is no significant acceleration in the middle of the plane after  $t = \tau_c$ . Some of the particles can get more acceleration traveling from other region to “hot spots”. Figure 4 *bottom* shows the distance particles traveled in  $z$  direction from its original places  $|z - z_0|$  versus time when particle get accelerated at a certain energy ( $p_c = 3p_0$ ). It shows many particles are accelerated close to their original position, which is related to the acceleration in the

“hot spot”. Nevertheless, there are also a number of particles travel from the connection point separating region to “hot spot” and get further acceleration, which is represented by the particles that travel a large distance in  $z$  direction.

Figure 5 shows the same plot as Figure 4, except here the critical momentum is  $p_c = 10.0p_0$ . It is shown again in Figure 5 *top* that most of particles are accelerated to high energy are in the hot spot. However, as opposite to Figure 4 *top*, there are very few particles accelerated at the center of plane since energetic particles more transport away from the middle region and the time available is not long enough. For a quick estimate, the acceleration time is approximately,

$$\begin{aligned} \tau_{acc} &= \frac{3}{U_1 - U_2} \int_{p_0}^p \left( \frac{\kappa_{pp1}}{U_1} + \frac{\kappa_{pp2}}{U_2} \right) d \ln p \\ &> \frac{3}{U_1 - U_2} \int_{p_0}^{10p_0} \left( \frac{\kappa_{\perp}}{U_1} + \frac{\kappa_{\perp}}{U_2} \right) d \ln p > \tau_c \end{aligned}$$

Therefore for most of particles, they do not have sufficient time to be accelerated to high energies at the center. A number of particles accelerated at the center will travel to the “hot spot” and get more acceleration, as shown in Figure 5 *bottom*.

Clearly, this presents different pictures of particle acceleration by the shock contain 2-D spatial magnetic field variations, indicates the resulting distribution function is spatially dependent. In Figure 6 we show the steady state energy spectra obtained in the regions *top*:  $[0.1 < x < 0.3, \pi - 0.2 < z < \pi]$  (black solid line), and  $[0.1 < x < 0.3, -0.1 < z < 0.1]$  (green dashed line) and *bottom*:  $[0.8 < x < 1.0, \pi - 0.2 < z < \pi]$  (black solid line), and  $[0.8 < x < 1.0, -0.1 < z < 0.1]$  (green dashed line). It is shown that the spatial difference among distribution functions at different locations caused by large-scale magnetic field variation is considerable. The black lines in both top plot and bottom plot, which correspond to the “hot spots”, show power-law like distributions except at high energies. At high energies, the particles will leave the simulation domain before gain enough energy which causes the roll over in distribution function, this roll over is mainly caused by a finite distance to upstream boundary. For other locations, the 2-D effect we discussed will produce the modification in distribution functions. The most pronounced effect can be found at the nose of the shock (green lines), in the top panel the distribution of which shows a suppression of acceleration at all the energies. This insufficient acceleration is most prominent in the range of  $6 - 12p_0$ . At these energies the acceleration time scales are longer than the time for the field line convection swipe the particles away from the connection-point separating region, as we discussed above. The bottom plot show that deep downstream the spectrum of accelerated particles is similar at high energies since the mobility of these particles.

### 3.2. An oblique shock

The previous discussion has established the effect of a spatially varying upstream magnetic field on the acceleration of fast charged particles at a shock which propagating normal to the average upstream magnetic field. We next consider the case where the shock propagation direction is *not* normal to the magnetic field.



Clearly, if the varying direction of the upstream magnetic field is such that at some places the local angle of the magnetic field relative to the average field direction exceeds the angle of the average magnetic field to the shock plane, we will have situations similar to that discussed in the previous sections. There will be places where the connection points of the magnetic field to the shock move further apart or closer together. Hence we expect the same physics can be applicable. An example is given in Figure 7. In this case the ratio of  $\delta B/B_0$  is taken to be 0.5, the averaged shock normal angle  $\theta_{Bn} = 70^\circ$ . It can be seen from this plot that the connection points can still move toward each other in some regions. Figure 8 shows the density contours of accelerated particles the same as Figure 2, but for the case of the oblique shock. We find that in this case the process we discussed in the last section is still persistent, even for a oblique shock and relative smaller  $\delta B/B_0$ . The “hot spot” forms correspond to the converging magnetic connection points and particle acceleration is suppressed in the region where connection points separate from each other. We may conclude that, for a shock which is oblique, if some magnetic field lines can intersect the shock multiple times, we have “hot spots” of accelerated particles forms where the connection points converging together.

#### 4. SUMMARY AND CONCLUSIONS

The acceleration of charged particles in shock waves is one of the most important unsolved problems in space physics and astrophysics. The charged particle transport in turbulent magnetic field and acceleration in shock region are two inseparable problems. In this paper we illustrate the effect of a large-scale sinusoidal magnetic field variation. This simple model allows a detailed examination of the physical effects. As the magnetic field lines pass through the shock, the connection points between field lines on the shock surface will move accordingly. We find that the region where connection points approaching each other will trap and preferentially accelerate particles to high energies and form “hot spots” along the shock surface, somewhat in analogy to the “hot spots” postulated by Jokipii & Kóta (2008). The shock acceleration will be suppressed at places where the connection points move apart each other. Some of the particles injected in those regions will transport to the “hot spots” and get further accelerated. The resulting distribution function is highly spatial dependent at the energies we studied, which could give a possible explanation to the *Voyager* observation of anomalous cosmic rays. Although we have discussed a simplified, illustrative model, the resulting spectra and radial distributions show qualitative similarity with the *in situ Voyager* observations. Thus, the

intensities do not in general, peak at the the shock and the energy spectra are not power laws. We show this process is robust even in the case of oblique shocks with relatively small magnetic field variations. Large scale magnetic field variation, which could be due to magnetic structures like magnetic clouds, or the ubiquitous large scale field line random walk, will strongly modify the simple planar shock solution. This effect could work in a number of situations for large scale shock acceleration including magnetic variations, for example, the solar wind termination shock and supernova blast waves.

#### ACKNOWLEDGEMENT

F. G. would like to thank Joe Giacalone for the tutorial and discussion of stochastic integration method. F. G. also thank Chunsheng Pei and Erica McEvoy for valuable discussion on stochastic differential equations. We acknowledge partial support from NASA under grants NNX08AH55G and NNX08AQ14G.

#### APPENDIX: STUDY DIFFUSIVE SHOCK ACCELERATION USING STOCHASTIC INTEGRATION METHOD

In a 2-D system we considered, the Parker transport equation (1) can be re-written as,

$$\frac{\partial f}{\partial t} = \frac{\partial}{\partial x} \left( \kappa_{xx} \frac{\partial f}{\partial x} + \kappa_{xz} \frac{\partial f}{\partial z} \right) + \frac{\partial}{\partial z} \left( \kappa_{xz} \frac{\partial f}{\partial x} + \kappa_{zz} \frac{\partial f}{\partial z} \right) - U_x \frac{\partial f}{\partial x} + \frac{1}{3} \frac{\partial U_x}{\partial x} \left[ \frac{\partial f}{\partial \ln p} \right] + Q \quad (3)$$

The equivalent stochastic differential equation is,

$$\Delta x = r_1 (2\kappa_{\perp} \Delta t)^{1/2} + r_3 (2(\kappa_{\parallel} - \kappa_{\perp}) \Delta t)^{1/2} \frac{B_x}{B} + U_x \Delta t + \left( \frac{\partial \kappa_{xx}}{\partial x} + \frac{\partial \kappa_{xz}}{\partial z} \right) \Delta t \quad (4)$$

$$\Delta z = r_2 (2\kappa_{\perp} \Delta t)^{1/2} + r_3 (2(\kappa_{\parallel} - \kappa_{\perp}) \Delta t)^{1/2} \frac{B_z}{B} + \left( \frac{\partial \kappa_{zz}}{\partial z} + \frac{\partial \kappa_{xz}}{\partial x} \right) \Delta t \quad (5)$$

$$\Delta p = \left( 1 - \frac{1}{3} \frac{\partial U_x}{\partial x} \right) \Delta t \quad (6)$$

Where  $r_1$ ,  $r_2$ , and  $r_3$  are different sets of random numbers which satisfy  $\langle r_i \rangle = 0$  and  $\langle r_i^2 \rangle = 1$ . In order to study diffusive shock acceleration, we approximate the shock layer as a sharp variation  $U_x = (U_1 + U_2)/2 - (U_1 - U_2) \tanh(x/th)/2$  with a thickness  $th$  much smaller compared with the characteristic length of diffusion acceleration  $\kappa_{xx1}/U_1$ . At the same time, we have to make sure the time step  $\Delta t$  is small enough to resolve the motion in the shock layer.

#### REFERENCES

- Axford, W. I., Leer, E., & Skadron, G. 1977, Proc. 15th ICRC, (Plovdiv), 11, 132  
 Bell, A. R. 1978, MNRAS, 182, 147  
 Blandford, R. D., & Ostriker, J. P. 1978, ApJ, 221, L29  
 Blandford, R., & Eichler, D. 1987, Phys. Rep., 154, 1  
 Cummings, A. C., Stone, E. C., McDonald, F. B., Heikkila, B. C., Lal, N., & Webber, W. R. 2008, in AIP Conf. Proc., 1039, Particle Acceleration and Transport in the Heliosphere and Beyond: 7th Annual International Astrophysics Conference (Melville, NY: AIP), 343  
 Florinski, V., & Zank, G. P. 2006, Geophys. Res. Lett., 33, 15110  
 Giacalone, J. and Jokipii, J.R., 1999, ApJ, 520, 204  
 Giacalone, J. 2005a, ApJ, 624, 765  
 Giacalone, J. 2005b, ApJ, 628, L37  
 Giacalone, J., & Neugebauer, M. 2008, ApJ, 673, 629  
 Guo, F., & Giacalone, J. 2010, ApJ, 715, 406  
 Kóta, J., & Jokipii, J. R. 2008, in AIP Conf. Proc., 1039, Particle Acceleration and Transport in the Heliosphere and Beyond: 7th Annual International Astrophysics Conference (Melville, NY: AIP), 397  
 Kóta, J. 2010, in preparation.  
 Krymsky, G. F. 1977, Akademiia Nauk SSSR Doklady, 234, 1306  
 Jokipii, J. R. 1966, ApJ, 146, 480  
 Jokipii, J. R., & Parker, E. N. 1969, ApJ, 155, 777

- Jokipii, J. R. 1971, *Reviews of Geophysics*, 9, 27
- Jokipii, J. R. 1982, *ApJ*, 255, 716
- Jokipii, J. R. 1987, *ApJ*, 313, 842
- Jokipii, J. R., & Kóta, J. 2008, in *AIP Conf. Proc.*, 1039, Particle Acceleration and Transport in the Heliosphere and Beyond: 7th Annual International Astrophysics Conference (Melville, NY: AIP), 390
- Li, G., & Zank, G. P. 2006, in *AIP Conf. Proc.*, 858, Physics of the Inner Heliosheath, ed. J. Heerikhuisen et al. (New York: AIP), 183
- Parker, E. N., 1965, *Planet. Space Sci.*, 13, 9
- Stone, E. C., Cummings, A. C., McDonald, F. B., Heikkila, B. C., Lal, N., & Webber, W. R. 2005, *Science*, 309, 2017
- Stone, E. C., Cummings, A. C., McDonald, F. B., Heikkila, B. C., Lal, N., & Webber, W. R. 2008, *Nature*, 454, 71
- McComas, D.J., and Schwadron, N. A., 2006, *Geophys. Res. Lett.*, 33, L024102
- Schwadron, N. A., Lee, M. A., & McComas, D. J. 2008, *ApJ*, 675, 1584
- Parker, E. N. 1979, Oxford, Clarendon Press; New York, Oxford University Press.

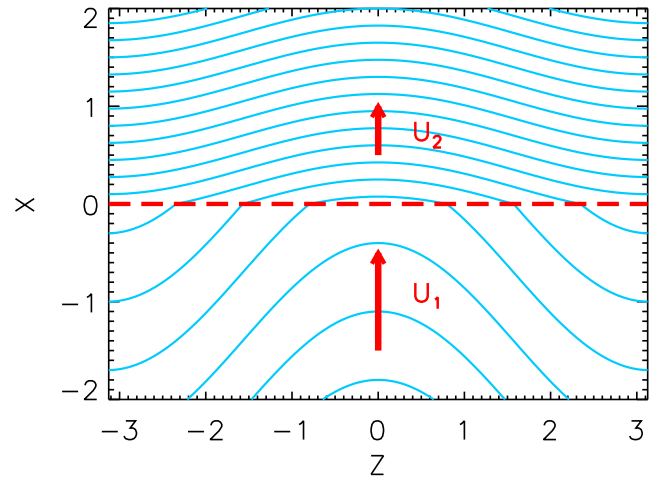


FIG. 1.— The shock and the magnetic field geometry for an upstream average magnetic field perpendicular to the shock normal. The blue lines represent the magnetic field lines and red dashed line indicates the surface of shock wave. The flow velocities are  $U_1$  (upstream) and  $U_2$  (downstream).

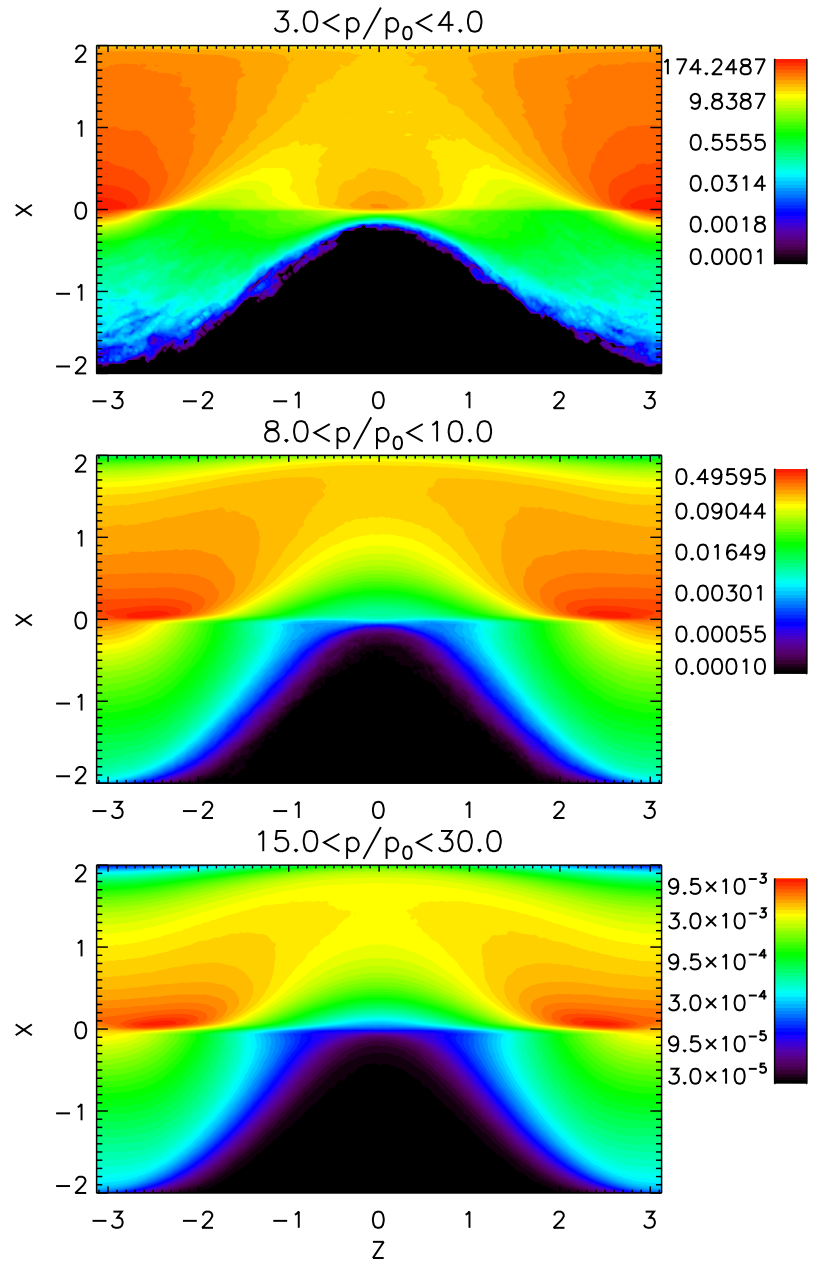


FIG. 2.— The representation of density contour of accelerated particles, for energy range:  $3.0 < p/p_0 < 4.0$  (top),  $8.0 < p/p_0 < 10.0$  (middle),  $15.0 < p/p_0 < 30.0$  (bottom). It is shown the hot spots forming on the both side of the system. The acceleration at the center of the shock is suppressed.

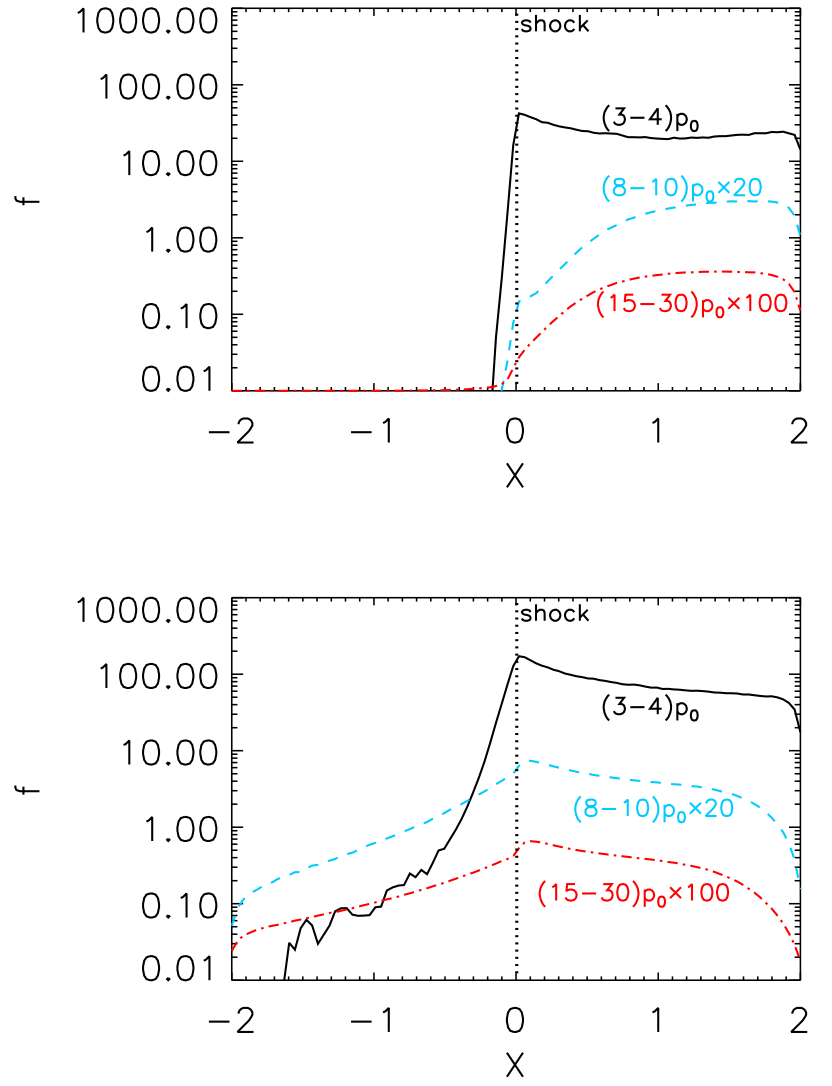


FIG. 3.— The profiles of density of the accelerated particles, for energy ranges:  $3.0 < p/p_0 < 4.0$  (black lines),  $8.0 < p/p_0 < 10.0$  (blue dashed lines),  $15.0 < p/p_0 < 30.0$  (red dot dashed lines) at different locations  $z = 0.0$  (top) and  $\pi$  (bottom), respectively.



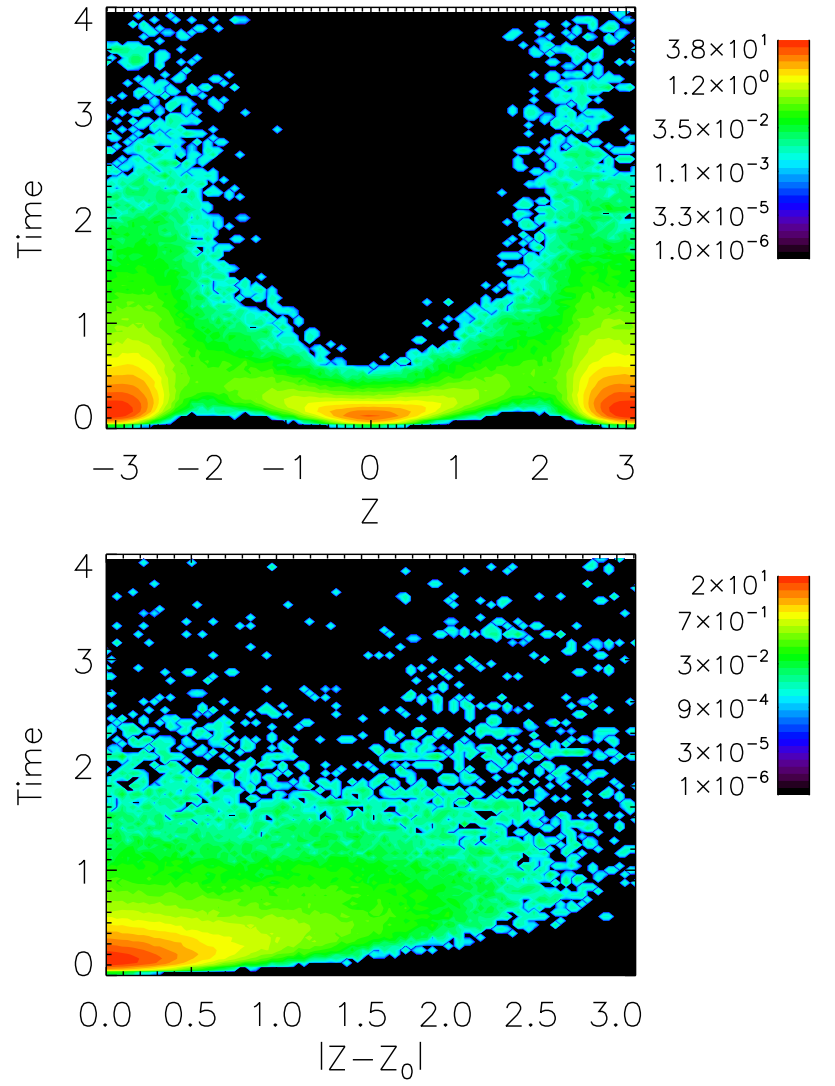


FIG. 4.— *top*: The position in  $z$  direction and time when the particle momentum reached  $p = 3.0p_0$ ; *bottom*: The travel distance in  $z$  direction  $|z - z_0|$  and time when the particle momentum reached  $p = 3.0p_0$ .

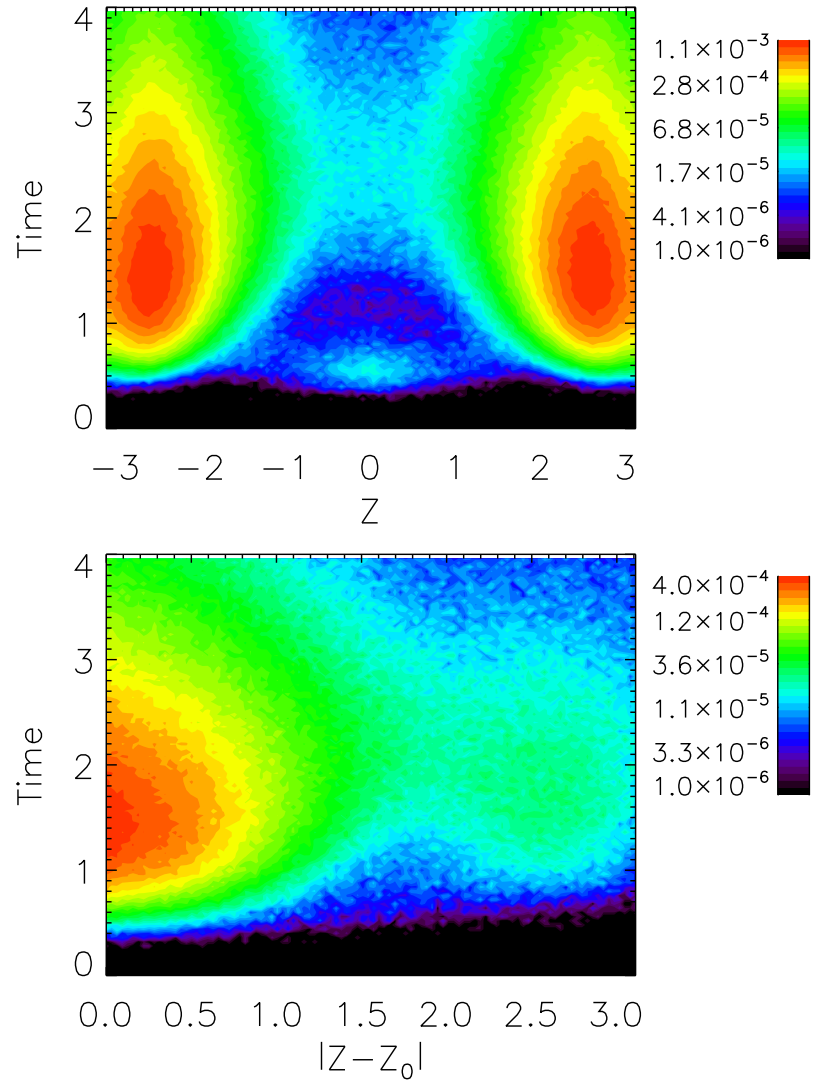


FIG. 5.— *top*: The position in  $z$  direction and time when the particle momentum reached  $p = 10.0p_0$ ; *bottom*: The travel distance in  $z$  direction  $|z - z_0|$  and time when the particle momentum reached  $p = 10.0p_0$ .

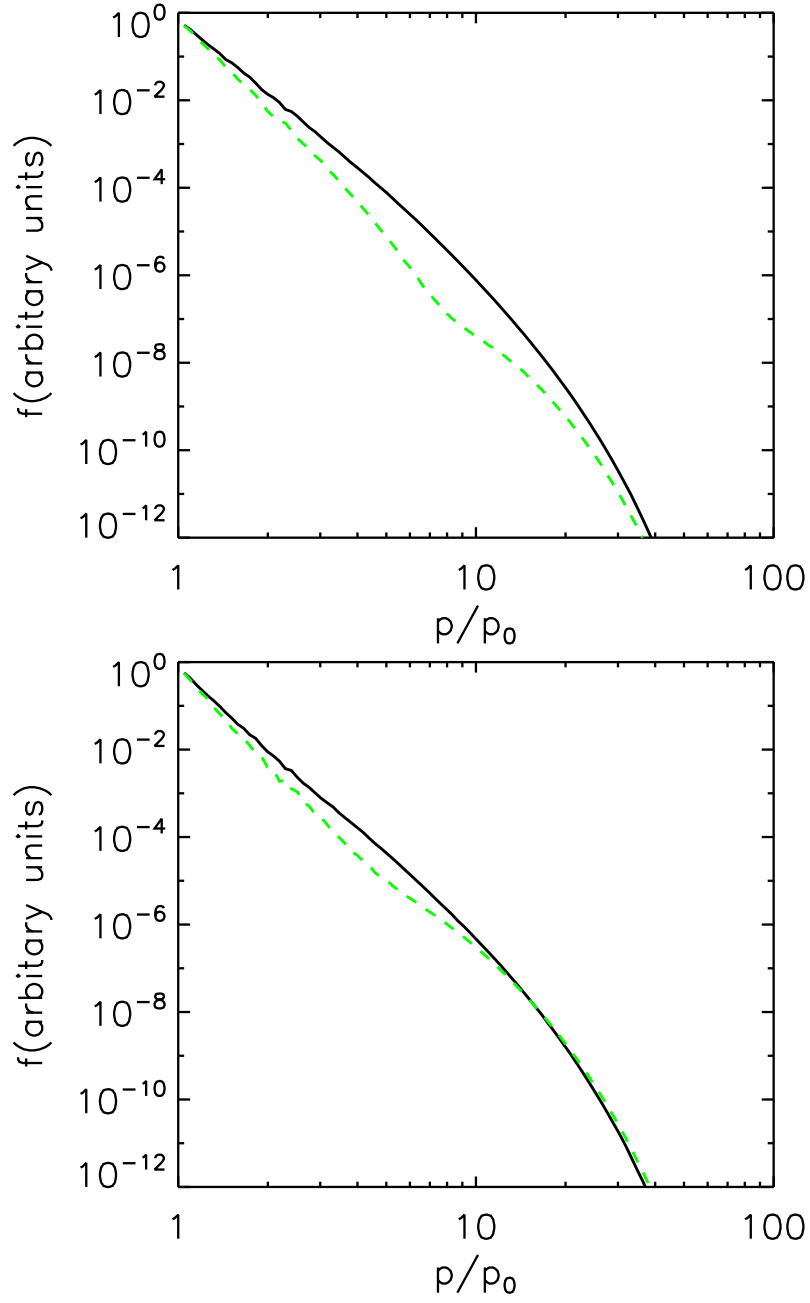


FIG. 6.— The steady state distribution functions at Top:  $[0.1 < x < 0.3, \pi - 0.2 < z < \pi]$  (black solid line),  $[0.1 < x < 0.3, -0.1 < z < 0.1]$  (green dashed line) and Bottom:  $[0.8 < x < 1.0, \pi - 0.2 < z < \pi]$  (black solid line),  $[0.8 < x < 1.0, -0.1 < z < 0.1]$  (green dashed line), respectively.

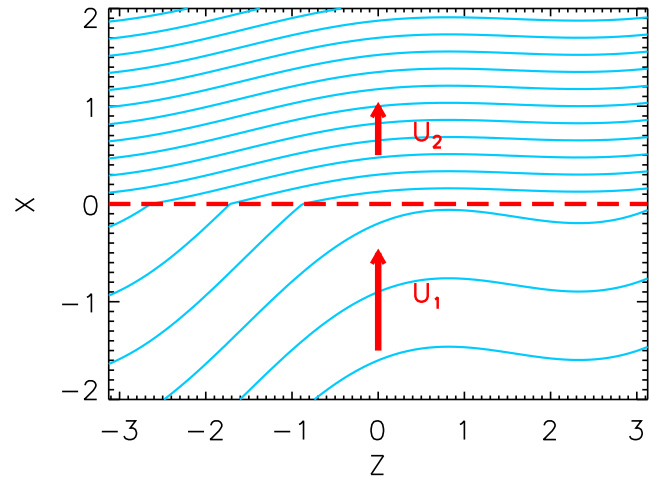


FIG. 7.— The shock and the magnetic field geometry considered for the case of an average magnetic field is  $70^\circ$  of the shock normal. The blue lines represent the magnetic field lines and red dashed line indicates the position of shock wave. The flow velocities are  $U_1$  (upstream) and  $U_2$  (downstream).

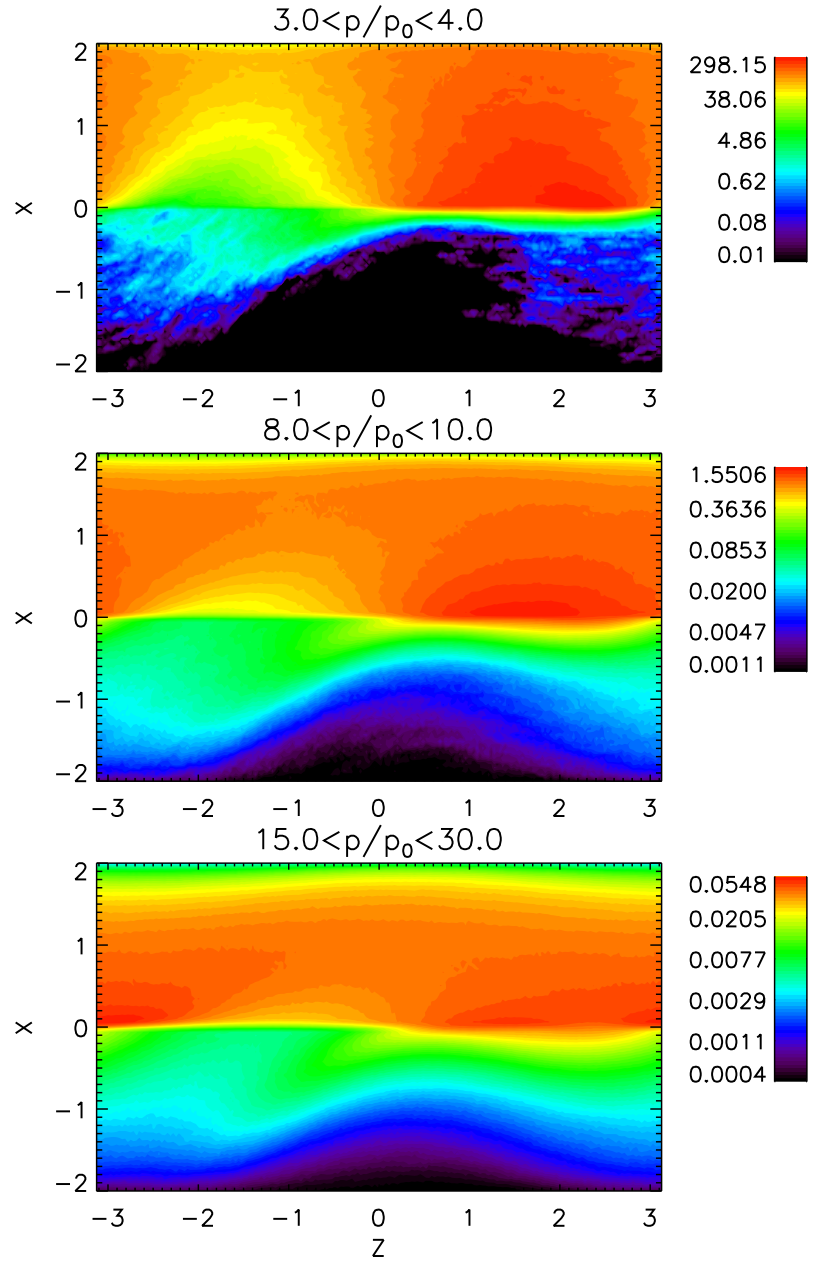


FIG. 8.— The density contour of accelerated particles in the case of oblique shock and  $\delta B/B_0 = 0.5$ , for energy range:  $3.0 < p/p_0 < 4.0$ (top),  $8.0 < p/p_0 < 10.0$ (middle),  $15.0 < p/p_0 < 30.0$ (bottom).